Original Research Article

Pharmacophore Based Virtual Screening and Docking of Different Aryl Sulfonamide Derivatives of 5HT₇R Antagonist

Nahid Fatema [1,2]

Vijjulatha Manga [2,3]

Lingala Yamini [3]

Salman Ahmad Khan [1]

Qasim Ullah [1*]

[1]Maulana Azad National Urdu University, Hyderabad, Telangana, India

[2]Department of Chemistry, Osmania University, Hyderabad, Telangana, India

[3]Osmania University College for Women, Hyderabad, Telangana, India

*email: drqasimullah@gmail.com

Abstract

The selective blockade of 5HT₇R (5-hydroxytryptamine 7 receptor) displays an antidepressant-like activity. It is a Gs-coupled receptor, which inactivates the adenyl cyclase enzyme or activates the potassium ion channel. Structural information of 5HT₇ was obtained by homology modeling using MODELLER v.9.13. In the present study, pharmacophore-based virtual screening, molecular docking, and binding free energy calculations were performed on a series of antagonist aryl sulphonamide derivatives. A five-point pharmacophore hypothesis with two hydrogen bond acceptor (A), one hydrogen bond donor (D), one positive group (p), and one ring (R) was developed with acceptable R^2 and Q^2 values of 0.90 and 0.602, respectively. Eventually, common pharmacophore hypothesis-based screening was conducted against Asinex databases. Finally, binding free energy and dock score analysis was carried out for the top hits obtained from the docking process. All 14 hits from the database in this study had a satisfactory dock score and binding energy values within the best active compound range. H bond interaction with amino acid residues Ser212 and π-π stacking with Tyr249 were investigated for the best active molecule. Both are present in the top hits, including other interactions as well.

INTRODUCTION

The 5-hydroxytryptamine 7 receptor (5HT₇R) was cloned in 1993 by independent laboratories[1,2]. This receptor, belonging to the G-protein-coupled receptor (GPCR) superfamily, is positively coupled to adenylate cyclase through the stimulatory Gαs proteins, and its activation results in an increase in cyclic adenosine monophosphate (cAMP). In addition, it has been recently demonstrated that the 5HT₇R interacts not only with the Gαs but also with Gα12 proteins[3]. 5HT₇ are Gαs-coupled heteroreceptors located in the limbic and cortical regions of the brain[4]. The typical antipsychotics, amisulpride, also acts as an antidepressant with a high-affinity 5HT₇R antagonist. Interestingly, the antidepressant-like behavioral effects of amisulpride are abolished in mice lacking 5HT₇R[5]. 5HT₇ receptor cDNAs have now been identified from several species (e.g., *Xenopus laevis* (toad), mouse, rat, guinea pig, and human[6]; homology modeling has been used to predict ligand action as part of pharmacophore modeling. The theoretical design of targeted ligands is hampered by the lack of the receptor's crystal structure.

Homology modeling (HM) can help with focused ligand design through theoretical screening and provide a solution. Homology modeling is one of the most widely used molecular modeling tools, allowing for predicting protein 3D

structures based on sequence similarity[7,8]. Rigid protein-flexible ligand docking was carried out using Glide in extra precision mode (GlideXP). The docking site used for validation includes the characteristic residues (Asp162, Cys166, Thr240, Ser243, Phe158, Phe344)[9].

Pharmacophore alignment and scoring engine (PHASE) was used to develop the 3D-QSAR models as a query in searching 3D databases containing "drug-like" small organic molecules and screened against the Asinex Elite synergy database in potency[10]. Unceasing our effort in developing potent $5HT_7R$ antagonists, we have recently done docking studies on the series of compounds [14-18] to obtain a five-point pharmacophore hypothesis AADPR. In order to identify potential hits, the hits obtained were subjected to a rigorous docking process, and drug-like candidates were screened for main interactions with target Human-$5HT_7$[11]. Using MM/GBSA, further binding energy calculations were also performed. All in all, an attempt was made in the present study to classify new $5HT_7$ receptors using integrated pharmacophore-based screening, molecular docking, and an approach to MM/GBSA.

The objective of the present study was to discover new potent inhibitors against $5HT_7$. Pharmacophore-based virtual screening, molecular docking, and binding-free analysis were employed to achieve this purpose. A five-point common pharmacophore hypothesis (AADPR) was developed using 61 $5HT_7R$ inhibitors and was applied to screen database Asinex macrocycles. The identified hits were docked into the active site of $5HT_7R$ and further subjected to binding free energy analysis.

MATERIALS AND METHODS

Hardware and Software

FASTA sequences were collected from https://www.ncbi.nlm.nih.gov/ Basic Local Alignment Search Tool (BLAST) to find the best template for modeling from the protein data bank (PDB) https://blast.ncbi.nlm.nih.gov/Blast.cgi. Homology models were generated using MODELLER v.9.13. PROCHECK, VERIFY3D, ProSA for protein validation. Schrödinger (2012), version 5.5. Schrödinger LLC, New York. QikProp module of Schrodinger.

Ligands

A stockpile of 61 molecules[9,12-15], aryl sulfonamide derivatives of (aryloxy) ethyl alicyclic amines compounds (**1-2**), aryl sulfonamide derivatives of (aryloxy) propyl piperidines compounds (**3-13**), azine sulfonamides of 4-[(2-ethyl)piperidinyl-1-yl] phenylpiperazines compounds (**14-26**), quinoline- and isoquinoline-sulfonamides and naphthalene sulfonamides compounds (**27-42**), quinoline- and isoquinoline-sulfonamides compounds (**43-45**), azine sulfonamides compounds (**46-49**) and sulfonamide alkyl (p-xylyl and benzyl) 1-(2-methoxyphenyl)piperazine (o-OMe-PhP) and 1-(2,3-dichlorophenyl)piperazine (2,3-DCPP) compounds (**51-61**) reported as $5HT_7$ receptor antagonist, and they were used to develop a three-dimensional pharmacophore model. The IC_{50} values of these derivatives were converted to the corresponding pIC_{50}. From a total of 61 compounds, 31 compounds were randomly chosen as a training set, and 30 compounds were selected as a test set in order to generate structural diversity in model generation. The structures of the derivatives taken in this study are represented in **Tables I** to **VI**.

Table I. Aryl sulfonamide derivatives of (aryloxy)ethyl alicyclic amines (**1-2**) and (aryloxy)propyl piperidines (**3-13**)
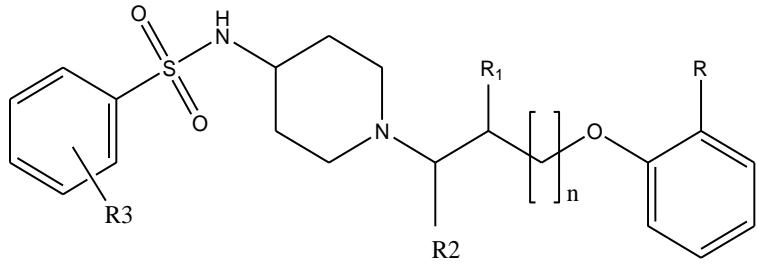
| Compounds	R	n	R_1	R_2	R_3
1	Isopropyl	0	H	H	4-F
2	Phenyl	0	H	H	3-Cl
3	Isopropyl	0	H	CH_3	3-F
4	Isopropyl	0	H	CH_3	4-F
5	Phenyl	0	H	CH_3	3-Cl

6	Phenyl	0	H	CH₃	4-F
7	Isopropyl	1	H	H	3-F
8	Isopropyl	1	H	H	4F
9	Phenyl	1	H	H	3-Cl
10	Phenyl	1	H	H	4-F
11	Isopropyl	1	OH	H	3-F
12	Isopropyl	1	OH	H	4-F
13	Phenyl	1	OH	H	3-Cl

Table II. Azine sulfonamides of 4-[(2-ethyl)piperidinyl-1-yl] phenylpiperazines (**14-26**)
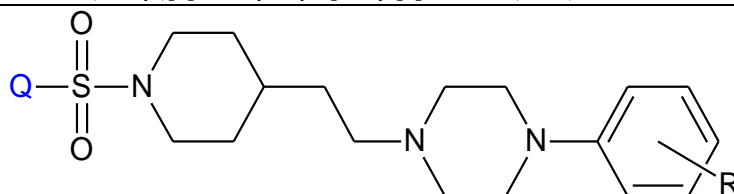
Compounds	Q	R
14	5-quinolinyl	H
15	4-isoquinolinyl	H
16	5-quinolinyl	4-Cl
17	4-isoquinolinyl	4-F
18	5-quinolinyl	3-Cl
19	4-isoquinolinyl	3-Cl
20	5-quinolinyl	3-F
21	4-isoquinolinyl	3-F
22	5-quinolinyl	3-3F₃
23	4-isoquinolinyl	3-3F₃
24	5-quinolinyl	2,3-DiCl
25	5-quinolinyl	3,4-DiCl
26	4-isoquinolinyl	3,4-DiCl

Table III. Quinoline- and isoquinoline-sulfonamides and naphthalene sulfonamides (**27-42**)

X=N,CH
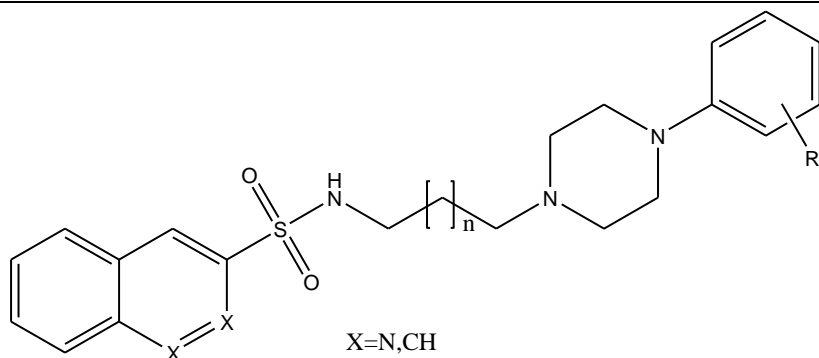
Compounds	Azinyl/naphthyl	n	R₁
27	3-quinolinyl	2	2-OCH₃
28	6-quinolinyl	2	2-OCH₃
29	8-quinolinyl	2	2-OCH₃
30	3-quinolinyl	1	4-Cl
31	4-isoquinolinyl	1	4-Cl
32	3-quinolinyl	2	3-Cl
33	6-Cl-3-quinolinyl	2	3-Cl
34	6-quinolinyl	2	3-Cl
35	8-quinolinyl	2	3-Cl
36	3-quinolinyl	2	4-Cl
37	6-quinolinyl	2	4-Cl
38	7-quinolinyl	2	4-Cl
39	4-isoquinolinyl	2	4-Cl
40	3-quinolinyl	3	4-Cl
41	1-naphthyl	2	3-Cl
42	2-naphthyl	2	3-Cl

Table IV.   Quinoline- and isoquinoline-sulfonamides (**43**-**45**)

X==N,CH
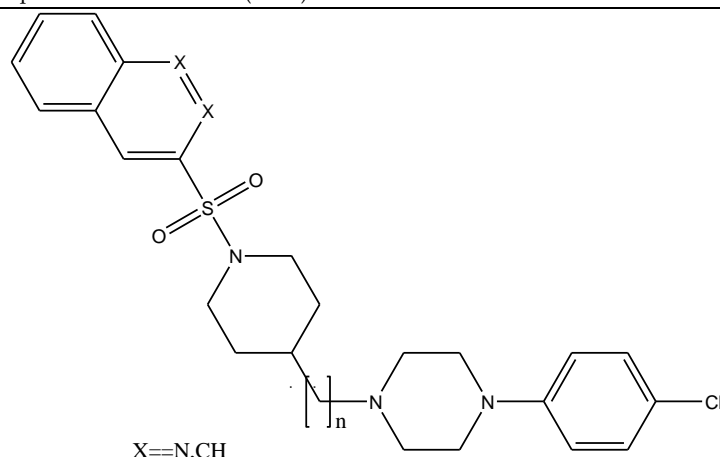
Compounds	Azinyl	n
43	3-quinolinyl	1
44	7-quinolinyl	1
45	3-quinolinyl	2

Table V.   Azine sulfonamides (**46-49**)

X=N
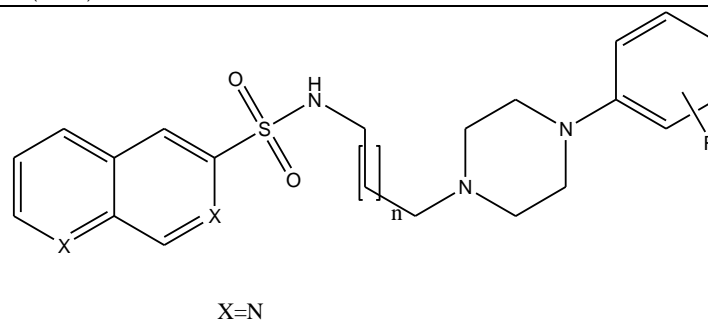
Compounds	Azinyl	n	R_1
46	3-isoquinolinyl	2	3-Cl
47	3-isoquinolinyl	2	2,3-diMe
48	7-quinolinyl	2	2,3-diCl
49	7-quinolinyl	1	2,3-diMe
50 **(Aripiprazole)**	-	-	-

Table VI.   Sulfonamide alkyl (p-xylyl and benzyl) 1-(2-methoxyphenyl) piperazine and 1-(2,3-dichlorophenyl) piperazine (**51-61**)
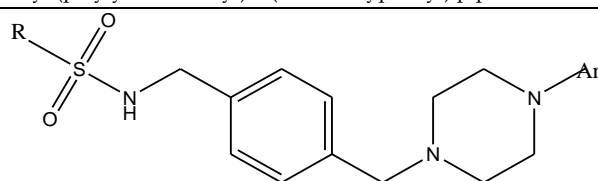
51-56=Ar=2-methoxyphenyl
57-61=Ar=2,3-dichlorophenyl   R=methyl,toluene,2-methylnapthalene

Compounds	R	n	Z
51	Toluene	1	SO_2
52	2-methylnaphthalene	1	SO_2
53	CH_3	1	SO_2
54	Toluene	0	SO_2
55	2-methylnapthalene	0	SO_2
56	CH_3	0	SO_2
57	Toluene	1	SO_2
58	2-methylnapthalene	1	SO_2

59	CH₃	1	SO₂
59	CH$_3$	1	SO$_2$
60	Toluene	0	SO$_2$
61	CH$_3$	0	SO$_2$

Receptors

During the study, no crystal structure data for the 5HT$_7$ receptor protein was available, so homology modeling of the human 5HT$_7$ was done using sequence information from the UniProt database (accession code: P34969)[17]. BLAST was performed to search the homologs, which serve as templates[18]. A template was selected based on the sequence identity, E value, and secondary structure similarities of the human 5HT$_7$R. Cluster X[19] was used to discover the conserved regions, identities, similarities, and differences between the target and the template using pairwise alignment. PDB ID 4XLR-m and 3PBL-a shared a sequence similarity of 90% with Human 5HT$_7$R. Low energy conformation of the protein structure of 5HT$_7$R was analyzed with PROCHECK[20], VERIFY3D[21], and ProSA[22] showed in a schematic workflow for homology modeling. The homology model was produced using MODELLER v.9.13[23] , with comparative modeling created by low-energy conformation. The modeled Human 5HT$_7$R is equivalent to a low-resolution X-ray crystal structure since the template and target proteins have higher than 80% sequence similarity[22]. This model was further used for docking studies.

Ligand Preparation

Total two-dimension structures were sketched in ChemSketch and ChemDraw and then converted to three-dimension structures before being subjected to ligand preparation using the LigPrep module[24]. A maximum of 100 conformers were generated per structure after the ligands were geometrically polished. Finally, at a physiological PH of 7±2, all potential low energy conformers were created, and their pIC$_{50}$ values were calculated and loaded into the Phase module.

Protein Preparation and Grid Generation

The modeled protein was utilized in this research. The Schrödinger suite's Protein Preparation Wizard module was used to create the appropriate protein crystal structures[25]. The modeled protein was subjected to the protein preparation process, review and modification, refinement, optimization, and minimization using the protein preparation wizard. Glide 5.6, used for docking around the active site of the protein. A receptor grid was generated by limiting the Vander Waals scale to 0.9[26]. Reported active sites of 5HT$_7$R were (Asp162, Val163, Phe343, Phe344, Gln235, Tyr239, Trp340, Ser347, and Agr357) as key amino acids residues by Zajdel *et al*[9].

Docking Studies

Docking studies were carried out using Schrödinger's docking protocol. It accounts for ligand flexibility with the docking program Glide. Rigid molecular docking experiments were used to screen and validate the designed pharmacophore, and results for the 5HT$_7$R complex were obtained. All ligands were prepared with LigPrep and optimized with the OPLS-2005 force field with a distance-dependent dielectric constant of 1.0 until a minimal energy difference of 0.001 kcal/mol was obtained as a convergence criterion[27]. To create mediated fit docking poses, we used van der Waals scaling of 0.7 and 0.5 for the receptor and ligand, respectively. Glide docking parameters were set to the default hard potential function during the re-docking stage, i.e., the van der Waals radii scaling is 1.0. The Glide XP was used for all docking calculations[28].

Docking-based Virtual Screening

The inhibitors attained from the Asinex database screening were docked within the binding site by the standard precision method. Then the top 10% scored ligand molecules were subjected to XP docking. To the top 10% scored ligands obtained from XP docking, the binding free energies were calculated using Prime MM/GBSA[29].

Prime/MMGBSA Calculations

Molecular Mechanics with Generalized Born Surface Area (MM/GBSA) is a method that uses a continuum solvent representation. Computationally, molecular dynamics simulations are costly nowadays. As a result, MM/GBSA is

used to calculate binding free energies because it is relatively affordable[30]. Then, using MM/GBSA and Prime from the Schrodinger suite, binding free energies for the top 17 hits from XP docking were determined. The complex energies for the dock positions derived from Glide and minimized from Prime were calculated using the OPLS-2005 force field[31]. The relative binding free energy (ΔG_{bind}) was calculated using the following **Equation 1**:

$$\Delta G_{bind} = G_{complex} - \left[G_{ligand(unbound)} + G_{receptor(unbound)} \right]$$
$$= \Delta E_{MM} + \Delta E_{Solv} + \Delta E_{SA} \dots [1]$$

ΔE_{MM} is the difference in energy between the protein-ligand complex and the sum of the protein's energies with and without ligand, while ΔG_{solv} is the difference between the protein-ligand complex's GBSA solvation energy and the total of the solvation energies for the unliganded protein and the ligand. ΔG_{SA} is defined as the difference between the surface energy of the protein-ligand complex and the sum of the surface area energies of the ligand and the unliganded protein. The VSGB 2.0 model was used in the Prime MM/GBSA computations. With an optimized tacit model, it equals the solvation-free energy[32]. The inner and exterior dielectric constants were set to 1 and 80, respectively, during the MM/GBSA calculations[33]. The VSGB model employs polarization and hydrophobic terms to illustrate polar and non-polar solute-solvent concentrations. The **Equation 2** could be used to project this, where f_{GB} stands for a function of generalized Born radii (ai and equation j) and distance between two atoms (ij).

$$G_{pol} = \frac{1}{2} \left(\frac{1}{\sum_{in}(ij)} - \frac{1}{\sum_{sol}} \right) \sum_{i<j} \frac{q_i q_j}{f_{GB}} \quad \dots [2]$$

RESULTS AND DISCUSSION

Four variant hypotheses were generated from the 31 training and 30 test set molecules, depicted in **Table VII** with IC_{50}, dock score, and fitness score. Total of fourteen variant combinations, viz. AADHR, AARRR, AAHRR, AADRR, AHRRR, AAPRR, APRRR, AADHP, HPRRR, ADHPR, AHPRR, ADPRR, AAHPR, and AADPR as popular pharmacophores were produced, each representing a balanced number of both more and less active molecules in the set. The geometry of AADPR is depicted in **Figure 1**, where the red sphere with vectors represents the H-bond acceptor feature (A2 and A3), the dark blue sphere with a vector represents the H-bond donor feature (D4), blue represents the positive group (P6), and one orange tori (ring-shaped surfaces) represents aromatic ring features (R9). Therefore atom-based 3D QSAR models were developed for the top fourteen pharmacophore hypotheses. PLS regression was performed with three maximum PLS factors where PHASE descriptions acted as independent variables while pIC_{50} values served as dependent variables. Therefore, it is evident that the developed 3D QSAR model has sterling statistical criteria and can be used for further optimization and exploration[34].

Table VII. 5HT$_7$ receptors and experimental and predicted pIC_{50} values of training and test set compounds based on pharmacophore hypothesis AADPR. Dock score and fitness score values of both best active (**1**) and least active (**30**) compounds are shown in bold

Compounds	Exp IC$_{50}$	Pred IC$_{50}$	Dock score	Fitness score
1	**9.52**	**9.52**	**-3.54**	**1.82**
2	8.15	8.29	-4.81	1.64
3	6.76	7.41	-3.90	1.85
4	7.13	7.85	-5.78	1.67
5	7.49	7.88	-4.39	1.76
6	7.46	7.81	-6.09	1.57
7	7.28	7.60	-2.85	1.84
8	7.49	7.30	-2.70	1.42
9	7.28	7.56	-5.01	1.74
10	7.23	7.72	-3.42	1.67
11	6.67	7.42	-6.04	1.75
12	6.98	7.70	-6.04	1.86
13	6.98	7.70	-6.04	1.84
14	6.67	7.09	-5.19	2.03

|				
15	6.75	7.09	-5.63	0.77
16	7.43	7.09	-5.38	2.02
17	7.85	7.79	-6.16	1.74
18	7.43	7.53	-5.82	1.71
19	7.74	7.79	-5.69	1.73
20	6.78	7.20	-5.51	1.69
21	6.84	7.09	-5.67	2.06
22	7.25	7.09	-6.91	1.97
23	7.28	7.09	-6.92	1.97
24	7.25	7.29	-6.25	1.72
25	7.28	7.43	-6.40	1.69
26	7.44	7.20	-0.80	1.69
27	7.10	7.30	-5.61	1.78
28	6.87	7.28	-6.72	1.71
29	7.25	7.31	-6.48	1.60
30	**6.21**	**7.42**	**-6.64**	**1.93**
31	6.94	7.42	-5.67	1.90
32	7.25	7.40	-6.91	1.87
33	7.03	7.45	-6.25	2.70
34	7.16	7.46	-6.581	1.76
35	7.60	7.44	-6.05	3.00
36	6.50	6.60	-5.93	0.91
37	6.47	6.60	-6.64	0.91
38	6.41	6.61	-6.00	0.93
39	7.16	7.44	-5.66	2.71
40	6.47	6.77	-6.28	1.22
41	7.44	7.10	-6.24	2.21
42	7.30	7.10	-6.41	2.11
43	6.83	7.06	-4.31	1.76
44	6.68	6.99	-5.82	1.82
45	7.39	7.45	-6.26	1.75
46	7.30	7.42	-6.25	2.52
47	7.07	7.52	-4.37	1.87
48	7.50	7.43	-6.22	1.79
49	7.92	7.52	-6.17	1.79
50 (Aripiprzole)	7.58	7.51	-6.18	2.07
51	6.64	6.79	-5.10	0.56
52	6.97	6.81	-6.70	1.10
53	6.34	6.42	-6.57	0.65
54	7.49	7.57	-3.68	2.05
55	7.92	8.34	-5.10	1.88
56	7.88	7.90	-3.83	2.06
57	6.67	7.03	-6.81	1.17
58	6.74	6.73	-6.63	0.77
59	6.50	6.44	-6.40	0.40
60	7.07	7.35	-6.09	2.00
61	8.09	7.68	-5.78	1.91
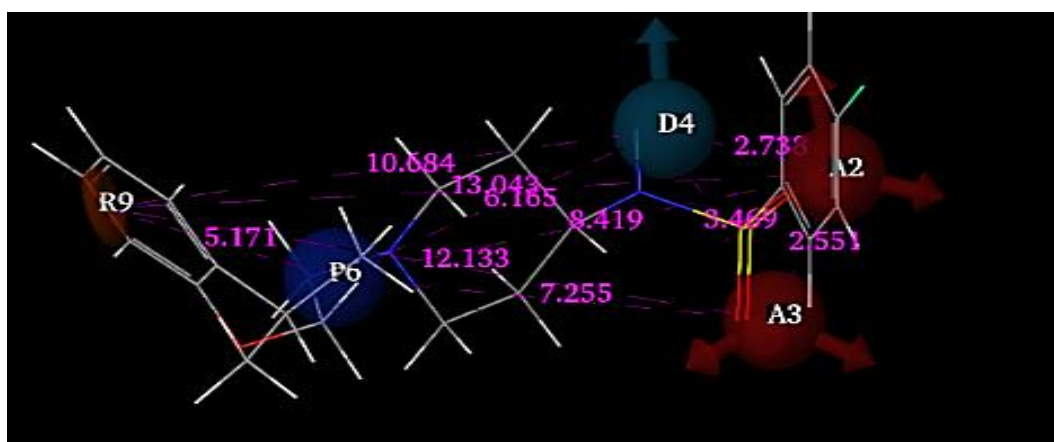
Figure 1. The illustration of pharmacophore model AADPR where the red sphere with vectors represents the H-bond acceptor feature (A2 and A3), the dark blue sphere with a vector represents the H-bond donor feature (D4), blue represents the positive group (P6), and one orange tori (ring-shaped surfaces) represents aromatic ring features (R9).

The scatter plot of experimental versus predicted pIC_{50} values of both training and test set ligands is shown in **Figure 2**. The graph showed a positive correlation between predicted and experimental values. Hence, it can be confirmed that the generated 3D QSAR model is significant.
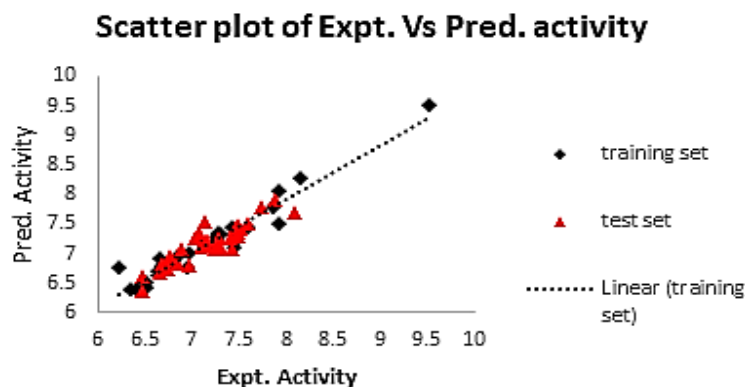

Figure 2. Scatter plot of experimental versus predicted pIC_{50} values of training and test set compounds derived from five-point (AADPR) hypothesis.

The hypothesis with the highest survival score was chosen for further investigation. Among the fourteen hypotheses, AADPR gave an excellent statistical model with high values of correlation coefficient; R^2 = 0.90, low standard deviation; SD = 0.518, variance ratio; F = 70.3, high predictive coefficient; Q^2 = 0.60, low RMSE = 0.336 and Pearson's R-value = 0.786 shown in **Table VIII** and it was discovered to have a five-point hypothesis with two hydrogen bond acceptors (AA), H-bond donor (D), positive group (P), aromatic ring (R). The hypothesis AADPR associated with five pharmacophore site points was taken for further analysis[35].

Table VIII. Atom based pharmacophore results

ID	SD	R^2	F	RMSE	Q^2	Pearson-R
AADPR	0.518	**0.9**	70.3	0.336	**0.60**	0.786

Model validation

The overall arrangement of helices and loops in the model is in good agreement with the corresponding elements in the X-ray structure of the template (PDB ID: 4XLR-m and 3PBL-a). The three-dimensional structure of homology modeled protein was validated using PROCHECK, VERIFY3D, and ProSA, as shown in **Figure 3**. First validation was performed using Ramachandran plot calculations computed with the PROCHECK program by checking the detailed stereochemical quality of each residue in the protein structure as shown in **Figure 4**. corresponds to the tertiary structure of $5HT_7$. A Ramachandran plot of phi (Φ) versus psi (ψ) for the modeled low energy conformer of $5HT_7$, along with plot statistics, is shown in **Figure 5**. Among 479 amino acids, 381 (90.5%) were in the most favored region, 36 residues in the additionally allowed region, three generously allowed, and one in the disallowed region, excluding glycine and proline. PROCHECK data showed the most promising results, confirming that the generated model was stereo chemically valid.
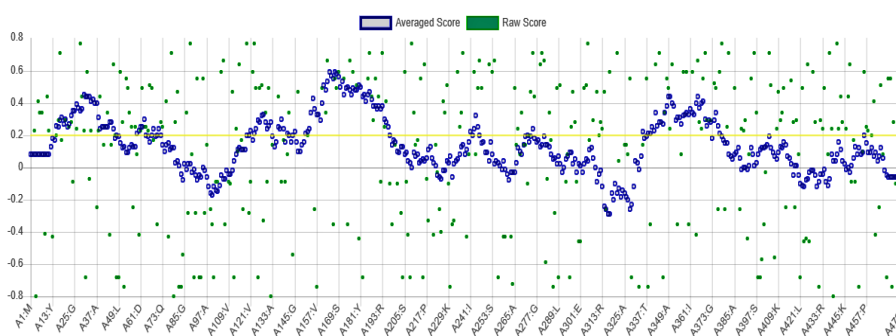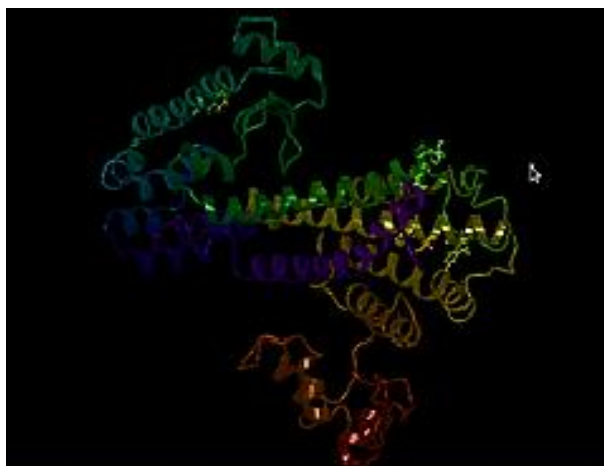

Figure 3. Verified 3D of modelled protein.
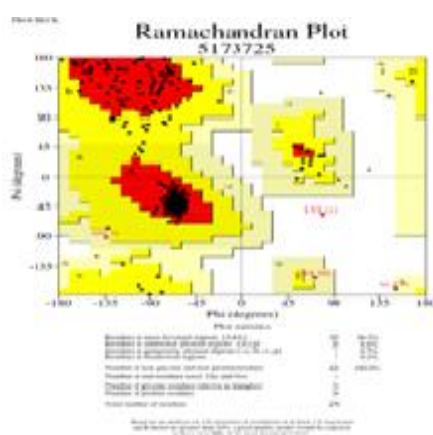
Figure 4. 5HT₇ modeled structure.

Figure 5. Ramachandran plot of modeled structure.

3D QSAR visualization of best active compound

Figures 6a to **6c** depict the 3D QSAR model visualization of the best active compound (**1**, pIC$_{50}$ = 9.52). The H-bond donor feature superposed on NH attached to the sulfonyl group is depicted in **Figure 6a**. It exactly matched the pharmacophoric feature, i.e., D4. On the other hand, H-bond acceptor features superposed on the oxygen atom of the sulfonyl group depicted in **Figure 6b** and benzene in **Figure 6c**. Interestingly, the hypothesis showed two H-bond acceptor features (A2, A3), which are very valuable for the activity.

a   b   c
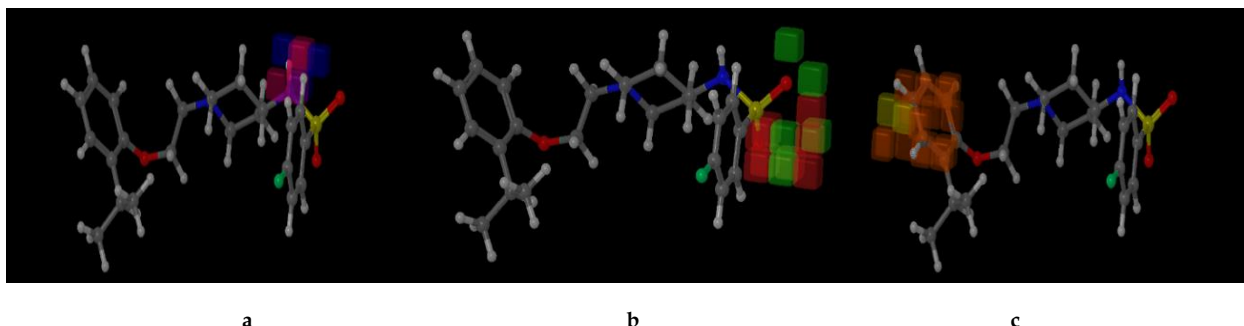
Figure 6. 3D QSAR model visualization in connection with the best active compound (**1**), illustrating the effect of acceptors-bond, donor, and R aromatic ring with pink (**a**), pale red (**b**), and orange (**c**) allowed regions respectively.

Virtual screening with pharmacophores

The hit molecules obtained from the database Asinex were docked into the active site of $5HT_7R$ using the receptor grid, which was generated during the docking process. The docking process was carried out in two stages in our analysis. About 1190 hits obtained from the Asinex macrocycles database were initially docked using SP mode. About 117 molecules (i.e., 10%) that showed high dock scores were passed on to the next stage of XP docking. The top 10%, i.e., 17 molecules of the Asinex macrocycles database, which exhibited good dock scores, were taken further for binding free energy analysis. The docking score of the top 10% of the hit molecules obtained from the Asinex database is shown in **Table IX**. These values were compared with the data set's dock score value of the best active compound **1** (**Table X**). From **Table IX**, it can be observed that all the hits showed good dock score values, which are in the good range compared to best active compound **1** (-3.543).

Table IX. H-bond interaction, binding free energies, dock score and predicted pIC_{50} values of screened hits obtained from Asinex macrocycles database (AX1-AX14) they are derivatives of 3-(1-methylpiperidin-3-yl)-1,2-oxazole-5-carboxamide AX1-AX6, 2-{4-[(6-oxo-1,6-dihydropyrimidin-2-yl) amino] piperidin-1-yl} acetamide AX7-AX9, N-[(piperidin-4-yl) methyl] acetamide AX10-AX13

Core structure (AX1-AX6)   Core structure (AX7-AX9)

Core structure (AX10-AX13)   AX14

S No	R_1	R_2	H-bond interaction	Binding energy (kcal/mol)	Dock score (xp)	pIC_{50}
AX1	1-fluoro-3-methylbenzene	Quinoline	Tyr 249	-80.79	-6.80	7.75
AX2	4-methylpyridine	Naphthalene	Ser 212	-67.74	-6.49	7.50
AX3	Ethyl	Naphthalene	Thr 244	-69.70	-6.15	7.77
AX4	4-methylpyridine	Quinoline	Tyr 249	-74.13	-5.72	7.57
AX5	Anisole	Quinoline	Tyr 249	-78.87	-5.76	7.34
AX6	1-fluoro-3-methylbenzene	Benzyl	Thr 249	-64.62	-5.73	7.88
AX7	4-CF_3	Naphthalene	Ser 212	-72.00	-5.62	7.28
AX8	4-ethyl	(trifluoromethyl)benzene	Ser 212	-65.63	-5.67	7.62
AX9	5,6-dimethyl	(trifluoromethyl)benzene	Ser 212	-66.21	-5.65	7.62
AX10	1,3,5-trimethyl-1*H*-pyrazole	3-(4-fluorophenyl)-1-methyl-1*H*-pyrazole	Tyr 249	-75.00	-5.95	7.35
AX11	2,5-dimethylpyrazine	3-(2-fluorophenyl)-1-methyl-1*H*-pyrazole	Ser 212	-74.16	-6.00	7.29
AX12	3-methylfuran	1-butyl-4-chlorobenzene	Ser 212 Thr 249	-71.69	-6.61	6.88
AX13	2-(propan-2-yl)-2*H*-benzotriazole n=1	Anisole	Tyr 249	-65.24	-5.76	6.95
AX14	-	-	Gln 455	-82.85	-6.07	7.51

Table X. The best active molecule with exp IC_{50}, pred IC_{50}, XP dock score, binding energy (kcal/mol), and fitness score

ExpIC_{50}	PredIC_{50}	XP-Dock score	Binding energy (kcal/mol)	Fitness score
9.522	9.52	-3.543	-57.312	1.82

Binding free energy analysis

The binding free energy values of the top 10% of the hit molecules obtained from the databases are shown in **Table X**. These values were compared with the binding free energy value of the best active compound **1** (**Table IX**). It can be observed that out of 17 molecules, 14 hits showed good binding free energy values. Molecules AX1, AX2, AX3, AX4, AX5, AX6, AX7, AX8, AX9, AX10, AX11, AX12, AX13, AX14, from Asinex macrocycles database in particular showed good binding energy values of -82.857, -80.792, -78.876, -75.007, -74.165, -74.138, -72.006, -71.690, -69.699, -67.746, -66.216, -65.636, -65.244, -64.627 kcal/mol respectively which are in the range of best active compound **1** (−57.312 kcal/mol).

Interaction study of screened hits

In interaction studies of screened hits, the ligand interaction diagram (LID) was employed to explore the interaction pattern of the screened hits[36]. The purple-colored lines in **Figure 7** represent hydrogen bonds, green-colored lines represent π-π stacking interactions, and red-colored lines represent π-cationic interactions. Initially, the best active compound in a complex with 5HT$_7$R was analyzed with the help of LID. It showed one hydrogen bond interaction with amino acid residues Ser212 and one π-π stacking with amino acid residue Tyr249. The hits obtained from Asinex database are derivatives of 3-(1-methylpiperidin-3-yl)-1,2-oxazole-5-carboxamide, 2-{4-[(6-oxo-1,6-dihydropyrimidin-2-yl) amino] piperidin-1-yl} acetamide, N-[(piperidin-4-yl) methyl] acetamide, showed π-π stacking, π cationic interactions apart from hydrogen bonds. They showed hydrogen bond interactions with Gln455, Tyr249, Ser212, Thr244, π-π stacking interactions with Thr249, Tyr242, Tyr249, and π-cationic interactions with Tyr249 and Trp462 shown in **Table X**. It is therefore clear that both linear and cyclic molecules can form interactions with 5HT$_7$ and may act as good inhibitors.
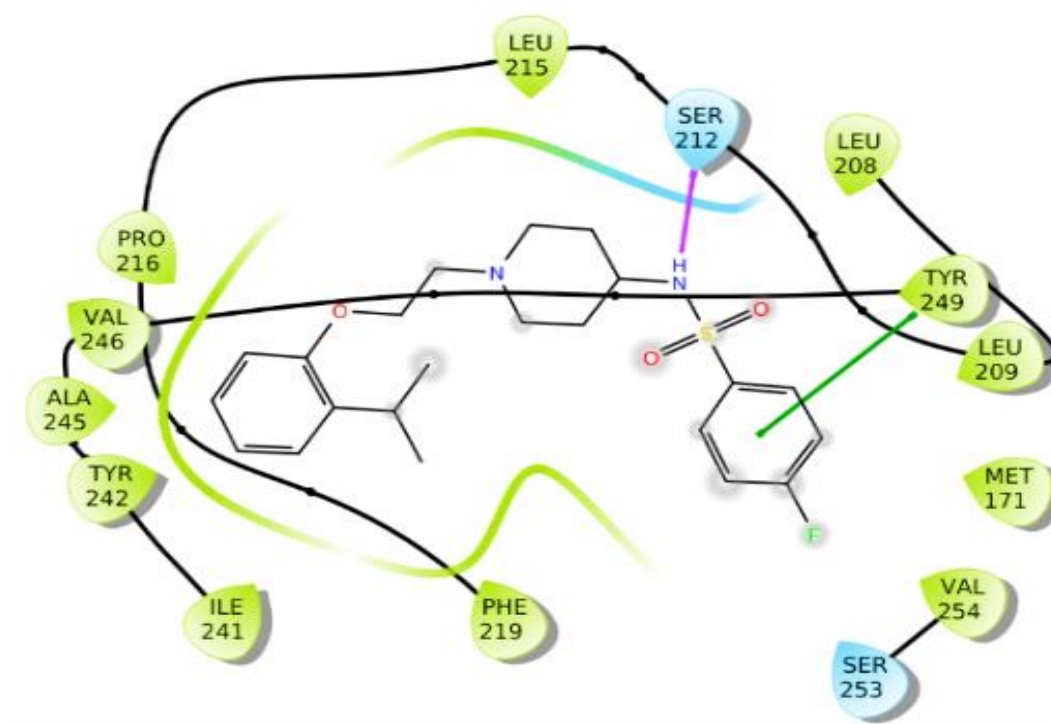

Figure 7. Ligand interaction diagram of a highest active compound **1**.

Prediction of ADME properties

By applying the QikProp module of Schrodinger, examining their physiochemical properties, and utilizing Lipinski's rule of five, screened compounds were evaluated for drug-likeness[37], as shown in **Table XI**. Lipinski's rule indicates that the molecule should exhibit drug-like properties H-bond donors <5, molecular weight <650 Daltons, H-bond acceptors <10, and a log p of <5. The water solubility (QPlogS) and partition coefficient (QPlogPo/w) for the screened

molecules is crucial for predicting drug absorption and distribution in the body, ranging from -2.34 to -4.45 and 0.91 to 4.52, respectively. Getting across the blood-brain barrier (BBB), which is required to enter a drug into the central nervous system (CNS), was found to be within acceptable limits. (-0.99 to 0.67), indicating that the compounds could be developed further for the treatment of depression. Caco-2 is a kind of cell. QPPCaco is a model that governs the gut-blood barrier[38] — varying from 60.59 to 702.07 MDCK Permeability of cells (QPPMDCK).

Table XI. ADME properties of screened molecules. a: screened molecule; b: predicted octanol/water partition coefficient log P (acceptable range -2.0 to 6.5); c: predicted aqueous solubility in mol/L (acceptable range -6.5 to 0.5); d: predicted Caco cell permeability in nm/s (acceptable range <25 is poor and >500 is great); e: predicted blood–brain barrier permeability (acceptable range -3 to 1.2); f: predicted apparent MDCK cell permeability in nm/s (acceptable range <25 is poor and >500 is great); g: percentage of human oral absorption (acceptable range 80% is high)

Molecule[a]	QPlogPo/w[b]	QPlogS[c]	QPPCaco[d]	QPlogBB[e]	QPPMDCK[f]	Percent human oral absorption[g]
AX1	4.43	-6.09	183.19	-0.56	157.88	93.43
AX2	4.01	-5.73	168.61	-0.73	79.91	90.31
AX3	3.80	-5.33	369.31	-0.28	186.48	95.16
AX4	3.32	-5.24	101.38	-0.99	46.11	8.30
AX5	4.09	-5.86	191.12	-0.67	91.49	91.76
AX6	4.52	-5.76	296.80	-0.35	265.24	100
AX7	3.09	-5.49	95.11	-0.73	199.19	80.48
AX8	2.57	-4.47	123.77	-0.62	201.98	79.44
AX9	2.63	-4.37	192.47	-0.29	340.80	83.25
AX10	4.33	-5.75	408.25	0.07	621.69	100
AX11	3.73	-5.37	343.14	-0.20	251.52	94.18
AX12	4.06	-5.39	154.73	-0.36	337.50	89.95
AX13	3.41	-4.18	456.41	-0.10	370.10	94.51
AX14	3.19	-2.66	189.76	0.40	100.45	86.44

CONCLUSION

The results revealed that the derivatives of 3-(1-methylpiperidin-3-yl)-1,2-oxazole-5-carboxamide, 2-{4-[(6-oxo-1,6-dihydropyrimidin-2-yl) amino] piperidin-1-yl} acetamide, N-[(piperidin-4-yl) methyl] acetamide, with prescribed pharmacophoric features can act as potent antagonist against 5HT$_7$R. Overall, the results obtained in this study suggest that the combined 3D QSAR, molecular docking, and binding free energy protocols can help identify new 5HT$_7$ receptors. We hope that the inferences drawn in this work can provide insights for researchers to discuss and design a new 5HT$_7$ receptor with greater activity.

ACKNOWLEDGMENT

CONFLICT OF INTEREST

The authors declare that there are no conflicts of interest.

FUNDING

DATA AVAILABILITY

All data are available from the authors.

AUTHORS' CONTRIBUTIONS

REFERENCES

1. Bard JA, Zgombick J, Adham N, Vaysse P, Branchek TA, Weinshank RL. Cloning of a novel human serotonin receptor (5-HT7) positively linked to adenylate cyclase. J Biol Chem. 1993;268(31):23422-6. doi:10.1016/S0021-9258(19)49479-9

2. Ruat M, Traiffort E, Leurs R, Tardivel-Lacombe J, Diaz J, Arrang JM, Schwartz JC. Molecular cloning, characterization and localization of a high-affinity serotonin receptor (5-HT7) activating cAMP formation. Proc Natl Acad Sci U S A. 1993;90(18):8547-51. doi:10.1073/pnas.90.18.8547

3. Kvachnina E, Liu G, Dityatev A, Renner U, Dumuis A, Richter DW, et al. 5-HT7 receptor is coupled to Gα subunits of heterotrimeric G12-protein to regulate gene transcription and neuronal morphology. J Neurosci. 2005;25(34):7821-30. doi:10.1523/JNEUROSCI.1790-05.2005

4. Renner U, Zeug A, Woehler A, Niebert M, Dityatev A, Dityateva G, et al. Heterodimerization of serotonin receptors 5-HT1A and 5-HT7 differentially regulates receptor signalling and trafficking. J Cell Sci. 2012;125(10):2486-99. doi:10.1242/jcs.101337

5. Abbas AI, Hedlund PB, Huang XP, Tran TB, Meltzer HY, Roth BL. Amisulpride is a potent 5-HT 7 antagonist: relevance for antidepressant actions in vivo. Psychopharmacology. 2009;205(1):119-28. doi:10.1007/s00213-009-1521-8

6. Lajoie Y, Teasdale N, Bard C, Fleury M. Attentional demands for static and dynamic equilibrium. Exp Brain Res. 1993;97(1):139-44. doi:10.1186/s13065-018-0422-5

7. Pramanik S, Kutzner A, Heese K. 3D Structure, Dimerization Modeling, and Lead Discovery by Ligand-protein Interaction Analysis of p60 Transcription Regulator Protein (p60TRP). Mol Inform. 2016;35(3-4):99-108. doi:10.1186/s13065-018-0422-5

8. Pramanik S, Kutzner A, Heese K. Lead discovery and in silico 3D structure modeling of tumorigenic FAM72A (p17). Tumour Biol. 2015;36(1):239-49. doi:10.1186/s13065-018-0422-5

9. Zajdel P, Marciniec K, Maślankiewicz A, Satała G, Duszyńska B, Bojarski AJ, et al. Quinoline-and isoquinoline-sulfonamide derivatives of LCAP as potent CNS multi-receptor—5-HT1A/5-HT2A/5-HT7 and D2/D3/D4—agents: The synthesis and pharmacological evaluation. Bioorg Med Chem. 2012;20(4):1545-56. doi:10.1016/j.bmc.2011.12.039

10. Vrontaki E, Kolocouris A. Pharmacophore Generation and 3D-QSAR model development using PHASE. Methods Mol Biol. 2018;1824:387-401. doi:10.1007/978-1-4939-8630-9_23

11. Hughes JP, Rees S, Kalindjian SB, Philpott KL. Principles of early drug discovery. Br J Pharmacol. 2011;162(6):1239-49. doi:10.1111/j.1476-5381.2010.01127.x

12. Partyka A, Kurczab R, Canale V, Satała G, Marciniec K, Pasierb A, et al. The impact of the halogen bonding on D2 and 5-HT1A/5-HT7 receptor activity of azinesulfonamides of 4-[(2-ethyl) piperidinyl-1-yl] phenylpiperazines with antipsychotic and antidepressant properties. Bioorg Med Chem. 2017;25(14):3638-48. doi:10.1016/j.bmc.2017.04.046

13. Marciniec K, Kurczab R, Książek M, Bębenek E, Chrobak E, Satała G, et al. Structural determinants influencing halogen bonding: a case study on azinesulfonamide analogs of aripiprazole as 5-HT 1A, 5-HT 7, and D 2 receptor ligands. Chem Cent J. 2018;12(1):55. doi:10.1093/nar/gkm290

14. Kowalski P, Śliwa P, Satała G, Kurczab R, Bartos I, Zuchowicz K. The effect of carboxamide/sulfonamide replacement in arylpiperazinylalkyl derivatives on activity to serotonin and dopamine receptors. Arch Pharm. 2017;350(10):1700090. doi:10.1002/ardp.201700090

15. Canale V, Partyka A, Kurczab R, Krawczyk M, Kos T, Satała G, et al. Novel 5-HT7R antagonists, arylsulfonamide derivatives of (aryloxy) propyl piperidines: add-on effect to the antidepressant activity of SSRI and DRI, and pro-cognitive profile. Bioorg Med Chem. 2017;25(10):2789-99. doi:10.1016/j.bmc.2017.03.057

16. Li J, Abel R, Zhu K, Cao Y, Zhao S, Friesner RA. The VSGB 2.0 model: a next generation energy model for high resolution protein structure modeling. Proteins. 2011;79(10):2794-812. doi:10.1002/prot.23106

17. Magrane M. UniProt Knowledgebase: a hub of integrated protein data. Database. 2011;2011:bar009. doi:10.1093/database/bar009

18. Johnson M, Zaretskaya I, Raytselis Y, Merezhuk Y, McGinnis S, Madden TL. NCBI BLAST: a better web interface. Nucleic Acids Res. 2008;36(Suppl 2):W5-9. doi:10.1093/nar/gkn201

19. Chenna R, Sugawara H, Koike T, Lopez R, Gibson TJ, Higgins DG, et al. Multiple sequence alignment with the Clustal series of programs. Nucleic Acids Res. 2003;31(13):3497–500. doi:10.1093/nar/gkg500

20. Laskowski RA, MacArthur MW, Moss DS, Thornton JM. PROCHECK: a program to check the stereochemical quality of protein structures. J Appl Cryst. 1993;26(2):283–91. doi:10.1107/S0021889892009944

21. Eisenberg D, Lüthy R, Bowie JU. VERIFY3D: assessment of protein models with three-dimensional profiles. Methods Enzymol. 1997;277:396–404. doi:10.1016/s0076-6879(97)77022-8

22. Wiederstein M, Sippl MJ. ProSA-web: interactive web service for the recognition of errors in three-dimensional structures of proteins. Nucleic Acids Res. 2007;35:W407–10. doi:10.1093/nar/gkm290

23. Kashif M, Hira SK, Upadhyaya A, Gupta U, Singh R, Paladhi A, et al. In silico studies and evaluation of antiparasitic role of a novel pyruvate phosphate dikinase inhibitor in Leishmania donovani infected macrophages. Int J Antimicrob Agents. 2019;53(4):508-14. doi:10.1016/j.ijantimicag.2018.12.011

24. Moussa N, Hassan A, Gharaghani S. Pharmacophore model, docking, QSAR, and molecular dynamics simulation studies of substituted cyclic imides and herbal medicines as COX-2 inhibitors. Heliyon. 2021;7(4):e06605. doi:10.1016/j.heliyon.2021.e06605

25. Peddi SR, Sivan SK, Manga V. Molecular dynamics and MM/GBSA-integrated protocol probing the correlation between biological activities and binding free energies of HIV-1 TAR RNA inhibitors. J Biomol Struct Dyn. 2018;36(2):486-503. doi:10.1080/07391102.2017.1281762

26. Friesner RA, Murphy RB, Repasky MP, Frye LL, Greenwood JR, Halgren TA, et al. Extra precision glide: Docking and scoring incorporating a model of hydrophobic enclosure for protein− ligand complexes. J Med Chem. 2006;49(21):6177-96. doi:10.1021/jm051256o

27. Debnath T, Majumdar S, Kalle AM, Aparna V, Debnath S. Identification of potent histone deacetylase 8 inhibitors using pharmacophore-based virtual screening, three-dimensional quantitative structure–activity relationship, and docking study. Res Rep Med Chem. 2015;5:21-39. doi:10.2147/RRMC.S81388

28. Kaushik AC, Kumar S, Wei DQ, Sahi S. Structure Based Virtual Screening Studies to Identify Novel Potential Compounds for GPR142 and Their Relative Dynamic Analysis for Study of Type 2 Diabetes. Front Chem. 2018;6:23. doi:10.3389/fchem.2018.00023

29. Bhowmick S, Saha A, Osman SM, Alasmary FA, Almutairi TM, Islam MA. Structure-based identification of SARS-CoV-2 main protease inhibitors from anti-viral specific chemical libraries: an exhaustive computational screening approach. Mol Divers. 2021;25(3):1979-97. doi:10.1007/s11030-021-10214-6

30. Genheden S, Ryde U. The MM/PBSA and MM/GBSA methods to estimate ligand-binding affinities. Expert Opin Drug Discov. 2015;10(5):449-61. doi:10.1517/17460441.2015.1032936

31. Rapp C, Kalyanaraman C, Schiffmiller A, Schoenbrun EL, Jacobson MP. A molecular mechanics approach to modeling protein-ligand interactions: relative binding affinities in congeneric series. J Chem Inf Model. 2011;51(9):2082-9. doi:10.1021/ci200033n

32. Mulakala C, Viswanadhan VN. Could MM-GBSA be accurate enough for calculation of absolute protein/ligand binding free energies? J Mol Graph Model. 2013;46:41-51. doi:10.1016/j.jmgm.2013.09.005

33. Kuchana V, Kashetti V, Peddi SK, Sivan S, Manga V. Integrated computational approach for in silico design of new purinyl pyridine derivatives as B-Raf kinase inhibitors. J Recept Signal Transduct Res. 2021:1-5. doi:10.1080/10799893.2021.1999472

34. Shehu Z, Uzairu A, Sagagi B. Quantitative structure activity relationship (QSAR) and molecular docking study of some pyrrolones antimalarial agents against plasmodium falciparum. J Turk Chem Soc Sect A Chem. 2018;5(2):569-84. doi:10.18596/jotcsa.346661

35. Le MT, Hoang VN, Nguyen DN, Bui THL, Phan TV, Huynh PNH, et al. Structure-Based Discovery of ABCG2 Inhibitors: A Homology Protein-Based Pharmacophore Modeling and Molecular Docking Approach. Molecules. 2021;26(11):3115. doi:10.3390/molecules26113115

36. Parker CG, Galmozzi A, Wang Y, Correia BE, Sasaki K, Joslyn CM, et al. Ligand and Target Discovery by Fragment-Based Screening in Human Cells. Cell. 2017;168(3):527-41. doi:10.1016/j.cell.2016.12.029

37. Jorgensen WL, Duffy EM. Prediction of drug solubility from structure. Adv Drug Deliv Rev. 2002;54(3):355-66. doi:10.1016/s0169-409x(02)00008-x

38. Itteboina R, Ballu S, Sivan SK, Manga V. Molecular modeling-driven approach for identification of Janus kinase 1 inhibitors through 3D-QSAR, docking and molecular dynamics simulations. J Recept Signal Transduct Res. 2017;37(5):453-69. doi:10.1080/10799893.2017.1328442